arXiv:astro-ph/0308518v1 28 Aug 2003

A Dearth of Dark Matter in Ordinary Elliptical Galaxies

Aaron J. Romanowsky,[1,2*] Nigel G. Douglas,[2] Magda Arnaboldi,[3,4] Konrad Kuijken,[5,2] Michael R. Merrifield,[1] Nicola R. Napolitano,[2] Massimo Capaccioli,[3,6] Kenneth C. Freeman[7]

[1]School of Physics & Astronomy, University of Nottingham, University Park, Nottingham, NG7 2RD, England

[2]Kapteyn Astronomical Institute, Postbus 800, 9700 AV Groningen, The Netherlands

[3]INAF-Astronomical Observatory of Capodimonte, via Moiariello 16, I-80131 Naples, Italy

[4]INAF-Astronomical Observatory of Pino Torinese, via Osservatorio 20, I-10025 Pino Torinese, Italy

[5]Leiden Observatory, Postbus 9513, 2300 RA Leiden, The Netherlands

[6]Department of Physical Sciences, University "Federico II", Naples, Italy

[7]Research School of Astronomy & Astrophysics, Mt. Stromlo Observatory, Cotter Road, Weston Creek, ACT 2611, Australia

[*]To whom correspondence should be addressed; E-mail: aaron.romanowsky@nottingham.ac.uk.

The kinematics of the outer parts of three intermediate-luminosity elliptical galaxies have been studied using the Planetary Nebula Spectrograph. The galaxies' velocity dispersion profiles are found to decline with radius; dynamical modeling of the data indicates the presence of little if any dark matter in these galaxies' halos. This surprising result conflicts with findings in other galaxy types, and poses a challenge to current galaxy formation theories.

Over the past twenty-five years, astronomers have gone from being surprised by the existence of dark matter to the understanding that in fact most of the Universe is dominated by exotic non-luminous material. In the prevailing paradigm, the gravitational influence of "cold

dark matter" (CDM) is crucial to the formation of structure, seeding the collapse and aggregation of today's luminous systems. An inherent consequence of this picture is that galaxies have massive, extended CDM halos. Indeed, such halos are evident around spiral galaxies, where the rotational speeds in their extended cold gas disks do not decrease outside the visible stars—a gravitational signature of dark matter (*1*).

The evidence for dark matter in elliptical galaxies is still circumstantial. Assessments of the total masses of individual elliptical systems have generally been confined to the very brightest ones, where the gravitational potential may be measured using x-ray emission (*2*) or strong gravitational lensing (*3*), and to nearby dwarfs, where the kinematics of individual stars offer a probe of the mass distribution (*4*). More "ordinary" elliptical galaxies, with luminosities close to the characteristic L^* (= $2.2\times10^{10} L_{B,\odot}$ in B-band solar units for a Hubble constant $H_0 = 70$ km s^{-1} Mpc^{-1}) (*5*), are more difficult to study because in general they lack a simple kinematical probe at the larger radii where dark matter is expected to dominate. The velocity distribution of the diffuse stellar light is the natural candidate (*6*), but studies have been limited by the faintness of galaxies' outer parts to radii $\lesssim 2R_{\rm eff}$ (where $R_{\rm eff}$ is the galaxy's "effective radius", enclosing half its projected light).

A powerful alternative is offered by planetary nebulae (PNe), which are detectable even in distant galaxies through their characteristic strong emission lines; once found, their line-of-sight velocities can then be readily determined by the Doppler shift in these lines. These objects have been used in the past as tracers of the stellar kinematics of galaxies (*7*), but the procedure of locating them using narrow-band imaging surveys and then blindly obtaining spectra at the identified positions has proved difficult to implement efficiently on a large scale. We have therefore developed a specialized instrument, the Planetary Nebula Spectrograph (PN.S), specifically to study the kinematics of PNe in elliptical galaxies (*8*). The PN.S uses counter-dispersed imaging (a type of slitless spectroscopy) over a wide field to simultaneously detect and measure velocities for PNe using their [O III] emission at 500.7 nm. Its optimization for this purpose means that the PN.S is far more efficient for extragalactic PN studies than any other existing instrumentation.

Observations with the PN.S on the 4.2-m William Herschel Telescope have allowed us to extend stellar kinematic studies to the outer parts of three intermediate-luminosity elliptical galaxies, NGC 821, NGC 3379, and NGC 4494 (Table 1). In each of these systems, we have measured ~ 100 PN velocities with uncertainties of 20 km s^{-1} out to radii of 4–6$R_{\rm eff}$ (Figs. 1–3). The line-of-sight velocities in the outer parts of all these galaxies show a clear decline in dispersion with radius (Fig. 4). A decrease in random velocities with radius has been indicated by small samples of PNe around NGC 3379 (*9*), but the more extensive data set presented here provides a more definitive measurement of this decline, and reveals that it also occurs in other similar galaxies. The new data are inconsistent with simple dark halo models (Fig. 4) and thus different from kinematical results for brighter ellipticals [e.g., (*6, 10*)].

More surprisingly, the velocity dispersion data follow simple models containing no dark matter (Fig. 4), showing the nearly Keplerian decline with radius outside 2 $R_{\rm eff}$ that such models predict, and suggesting that these systems are not embedded in massive dark halos. However,

a declining profile can also be the signature of a distribution of orbits that is primarily radial, because the observable line-of-sight component of velocity in such a system will decline with radius even if the magnitude of the velocity remains constant due to a surrounding dark halo. To assess the impact of this well-known degeneracy between mass and orbital anisotropy, we have constructed spherical Jeans models (see Appendix) with a fixed anisotropy, spanning a range from radially- to tangentially-biased extremes. We have fitted these models to the observed velocity dispersion profiles for the stars (*11,12,13*) and the PNe, inferring a benchmark quantity Υ_{B5}, the B-band mass-to-light ratio in solar units at 5 $R_{\rm eff}$ (Table 1). Even with this extra degree of freedom in the modeling, the values of 5–17 are low compared with the typical Υ_{B5} of $\sim$ 20–40 found for bright elliptical galaxies (*2,14*).

These models are not completely definitive, as there is no physical reason why the orbital anisotropy should not vary with radius. But we also have not used all the information contained in the kinematical data, fitting only binned root-mean-square values of the stellar and PN velocities, rather than the full two-dimensional distribution of line-of-sight velocities as a function of projected radius. To overcome these remaining limitations, we have used an orbit library method (see App.) to model the dynamics of NGC 3379. This procedure takes a broad suite of parameterized mass models, allows for orbital anisotropies that vary arbitrarily with radius, and finds the best fit to the PN velocity data as well as to the stellar brightness distribution (*15*) and kinematics (*12*), including the higher-order velocity moments that quantify the shape of the velocity distribution.

This procedure's only underlying assumptions are that Newtonian gravity applies, that the galaxy is in equilibrium, and that it is spherically symmetric. With respect to the latter assumption, the observed ellipticity of NGC 3379 varies from 0.14 to 0.30, so that its gravitational potential can be approximated as spherical to better than 10% accuracy. More serious is the possibility that this system contains a face-on disk component similar to an S0 galaxy, as has been suggested for faint ellipticals in general (*16*) and for NGC 3379 in particular (*15*); such a cold component could be responsible for the apparent low velocities. However, kinematical modeling of the inner regions (*17*) and the weak rotation of the outer parts indicate that this is unlikely; furthermore, the galaxy's globular cluster system also shows a steeply declining dispersion profile (*18*), and this population is unlikely to contain a disk component. The model also relies on the PNe following the same spatial and velocity distribution as the main stellar component; this is not strictly true because oxygen abundance radial gradients make the PN detectability vary with radius, but we calculate that this will cause a mass underestimate of only $\sim$ 5%. Another potential complication is that background emission-line galaxies can masquerade as PNe. We have discarded several of these from the data set on the basis of their extended appearance, and one that is a $>$3-σ outlier; any remaining contaminants would cause an apparent increase in the velocity dispersion at large radii, which is not seen in the data so the sample does not appear to be significantly contaminated. Within these assumptions, the modeling process should uncover the range of possible combinations of mass and orbit distribution that could reproduce the galaxy's observed properties.

Using this method to analyze the data for NGC 3379 (Fig. A1) reveals that Υ_{B5} is tightly constrained to be only 6.4 ± 0.6. Because population synthesis models indicate that the stars of NGC 3379 have $\Upsilon_{B\star} =$ 4–9 (*19*), and dynamical models of the inner regions where little dark matter is expected indicate $\Upsilon_{B\star}$ =6–7 (*20*), this result suggests a "naked" galaxy with no dark matter cloaking its visible body. However, the mass distribution inferred by this modeling process does not quite match the light distribution (Fig. A2), so there appears to be a small amount of dark matter. A dark matter-less galaxy is still possible if the baryonic Υ_B varies somewhat with radius, due to a gradient in the properties of the stellar population, or due to the presence of some undetectable baryonic component such as warm hydrogen gas. Such models may be plausible but are also somewhat *ad hoc*. In any case, the ratio of dark matter to total mass within 5 $R_{\rm eff}$ (9 kpc) is $\leq$ 0.32, so the galaxy within this region is not dark matter dominated. Extrapolating the models to the virial radius (120 kpc), we find $\Upsilon_B = 32 \pm 13$, which is consistent with the value of $\Upsilon_B = 27 \pm 5$ found by an independent analysis of the kinematics of a cold gas ring at 110 kpc (*21*).

Out of the five intermediate-luminosity ellipticals studied to date with extended kinematics [the three from this study as well as NGC 2434 (*22*) and NGC 4697 (*23*)], four have declining velocity dispersions. The fourth, NGC 4697, has $\Upsilon_{B5} \sim 11$ from Jeans modeling, so all four galaxies are consistent with $\Upsilon_{B5} \lesssim 13$. The apparent low dark matter content in these systems could be explained by pathological orbit structures (such as rapid strong anisotropy variations with radius), but the orbit library analysis rules out this possibility for NGC 3379, and in general such behavior has not been found in similar detailed modeling of elliptical galaxies. Latent disks could be to blame, but as with NGC 3379, the observed rotational speeds are low, and hiding them adequately would require coincidentally unpropitious viewing angles. Thus it seems most plausible that the apparent Keplerian decline in the velocity dispersions of all these systems is what it seems to be, and many ordinary elliptical galaxies are highly deficient in dark matter relative to other galaxy types—a possibility already hinted at by previous dynamical studies (*24, 19, 25*).

This result clashes with conventional conceptions of galaxy formation: in particular, if ellipticals are built up by mergers of smaller galaxies, it is puzzling for the resulting systems to show little trace of their precursors' dark matter halos. More detailed comparisons with the predictions of the standard CDM paradigm are not yet possible, because the baryonic processes during galaxy formation are complex, and high-resolution *ab initio* simulations are so far unable to reproduce an elliptical galaxy. However, estimating the effects of baryonic collapse on a CDM halo (*26*) using an adiabatic approximation yields $\Upsilon_{B5} \sim 20$. Low resolution simulations including baryonic processes (*27*), extrapolated inward in radius, also predict $\Upsilon_{B5} \sim 20$. These values conflict with those derived for the observed galaxies above. On the other hand, CDM predictions at the virial radius are generally supported by statistical studies of L^* ellipticals using weak gravitational lensing (*28*). This apparent disparity could be resolved if the dark matter content of ellipticals varies, or if these galaxies have large amounts of dark matter spread out to still larger radii than the PNe can probe. The former scenario begs a suitable mechanism for dark matter depletion, and the latter violates CDM predictions for high central concentrations

of dark halos—a problem that is also increasingly evident in other stellar systems (*29*).

It is apparent that some important physics is still missing from the recipes for galaxy formation. One obvious candidate is that substantial portions of these galaxies' dark matter halos have been shed through interactions with other galaxies. Such stripping has been inferred for ellipticals near the centers of dense galaxy clusters (*30*), but the galaxies we studied here are in much sparser environments, where substantial stripping is not expected to have been an important process. Crucial to understanding the incidence and origin of this low dark matter phenomenon will be results for a large sample of ellipticals with a broad range of properties, including differing environmental densities, which could be a key factor in determining halo outcomes; the continuing PN.S observing program will provide this sample.

References and Notes

1. M. Persic, P. Salucci, F. Stel, *Mon. Not. R. Astron. Soc.* **281**, 27 (1996).

2. M. Loewenstein, R. E. White III., *Astrophys. J.* **518**, 50 (1999).

3. C. R. Keeton, *Astrophys. J.* **561**, 46 (2001).

4. J. Kleyna, M. I. Wilkinson, N. W. Evans, G. Gilmore, C. Frayn, *Mon. Not. R. Astron. Soc.* **330**, 792 (2002).

5. D. S. Madgwick *et al.*, *Mon. Not. R. Astron. Soc.* **333**, 133 (2002).

6. A. Kronawitter, R. P. Saglia, O. Gerhard, R. Bender, *Astron. Astrophys. Suppl. Ser.* **144**, 53 (2000).

7. X. Hui, H. C. Ford, K. C. Freeman, M. A. Dopita, *Astrophys. J.* **449**, 592 (1995).

8. N. G. Douglas *et al.*, *Publ. Astron. Soc. Pac.* **114**, 1234 (2002).

9. R. Ciardullo, G. H. Jacoby, H. B. Dejonghe, *Astrophys. J.* **414**, 454 (1993).

10. J. Magorrian, D. Ballantyne, *Mon. Not. R. Astron. Soc.* **322**, 702 (2001).

11. R. Jedrzejewski, P. L. Schechter, *Astron. J.* **98**, 147 (1989).

12. T. S. Statler, T. Smecker-Hane, *Astrophys. J.* **117**, 839 (1999).

13. R. Bender, R. P. Saglia, O. E. Gerhard, *Mon. Not. R. Astron. Soc.* **269**, 785 (1994).

14. N. A. Bahcall, L. M. Lubin, *Astrophys. J.* **447**, L81 (1995).

15. M. Capaccioli, E. V. Held, H. Lorenz, M. Vietri, *Astron. J.* **99**, 1813 (1990).

16. H.-W. Rix, C. M. Carollo, K. Freeman, *Astrophys. J.* **513**, L25 (1999).

17. T. S. Statler, *Astron. J.* **121**, 244 (2001).

18. M. A. Beasley, T. J. Bridges, D. A. Forbes, in preparation (2003).

19. O. Gerhard, A. Kronawitter, R. P. Saglia, R. Bender, *Astronom. J.* **121**, 1936 (2001).

20. K. Gebhardt *et al.*, *Astronom. J.* **119**, 1157 (2000).

21. S. E. Schneider, *et al.*, *Astronom. J.* **97**, 666 (1989).

22. H.-W. Rix, P. T. de Zeeuw, N. Cretton, R. P. van der Marel, C. M. Carollo, *Astrophys. J.* **488**, 702 (1997).

23. R. H. Méndez *et al.*, *Astrophys. J.* **563**, 135 (2001).

24. G. Bertin *et al.*, *Astron. Astrophys.* **292**, 381 (1994).

25. M. Capaccioli, N. R. Napolitano, M. Arnaboldi, in *Proc. Sakharov Conf. of Physics*, in press (available at http://xxx.lanl.gov/abs/astro-ph/0211323).

26. J. F. Navarro, C. S. Frenk, S. D. M. White, *Astrophys. J.* **490**, 493 (1997).

27. D. H. Weinberg, R. Davé, N. Katz, L. Hernquist, *Astrophys. J.*, submitted (available at http://xxx.lanl.gov/abs/astro-ph/0212356).

28. G. Wilson, N. Kaiser, G. A. Luppino, L. L. Cowie, *Astrophys. J.* **555**, 572 (2001).

29. J. P. Ostriker, P. Steinhardt, *Science* **300**, 1909 (2003).

30. P. Natarajan, J.-P. Kneib, I. Smail, *Astrophys. J.* **580**, L11 (2002).

31. J. L. Tonry *et al.*, *Astrophys. J.* **546**, 681 (2001).

32. G. de Vaucouleurs, *et al.*, *Third Reference Catalogue of Bright Galaxies* (Springer-Verlag, New York, 1991).

33. S. M. Faber, *et al.*, *Astrophys. J. Suppl. Ser.* **69**, 763 (1989).

34. G. H. Jacoby, R. Ciardullo, W. E. Harris, *Astrophys. J.* **462**, 1 (1996).

35. The compressed files of the “Palomar Observatory - Space Telescope Science Institute Digital Sky Survey” of the northern sky, based on scans of the Second Palomar Sky Survey are copyright (c) 1993-2000 by the California Institute of Technology. Produced under Contract No. NAS5-2555 with the National Aeronautics and Space Administration.

Galaxy	Type	D (Mpc)	$R_{\rm eff}$	M_B	Observations	N(PNe)	Υ_{B5} ($\Upsilon_{B,\odot}$)
NGC 821	E2	24	50″	-20.5	Sep 01, 11h	104	13–17
NGC 3379	E1	11	35″	-20.0	Mar 02, 3h	109	5–8
NGC 4494	E0	17	49″	-20.6	Mar 02, 4h	73	5–7

Table 1: Properties of three galaxies observed with the Planetary Nebula Spectrograph. Columns show galaxy name, type, distance (*31*), effective radius (*32*), absolute magnitude, date and effective integration time of observations (normalized to 1″ seeing), number of PNe detected, and the range of *B*-band mass-to-light ratio at 5 effective radii (in solar units) determined from anisotropic Jeans models. The mass-to-light ratios are systematically sensitive to the assumed distance—e.g., if $D = 33$ Mpc for NGC 821 (*33*), Υ_{B5} is decreased by 30%; and if $D =$ 11–13 Mpc for NGC 4494 (*33, 34*), Υ_{B5} is increased by 30–60%. The characteristic magnitude is M_B^* = -20.4 (*5*).

36. J. Binney, S. Tremaine, *Galactic Dynamics* (Princeton Univ. Press, Princeton, PA, 1987), sec. 4.2.

37. L. Hernquist, *Astrophys. J.* **356**, 359 (1990).

38. A. J. Romanowsky, C. S. Kochanek, *Astrophys. J.* **553**, 722 (2001).

39. Based on observations made with the William Herschel Telescope operated on the island of La Palma by the Isaac Newton Group in the Spanish Observatorio del Roque de los Muchachos of the Instituto de Astrofisica de Canarias. Use was made of the HyperLeda galaxy database: http://www-obs.univ-lyon1.fr/hypercat/ . We thank Ortwin Gerhard and the anonymous referee for their helpful comments for improving the paper. NRN is supported by the European Commision FP5 Marie Curie Fellowships Programme.

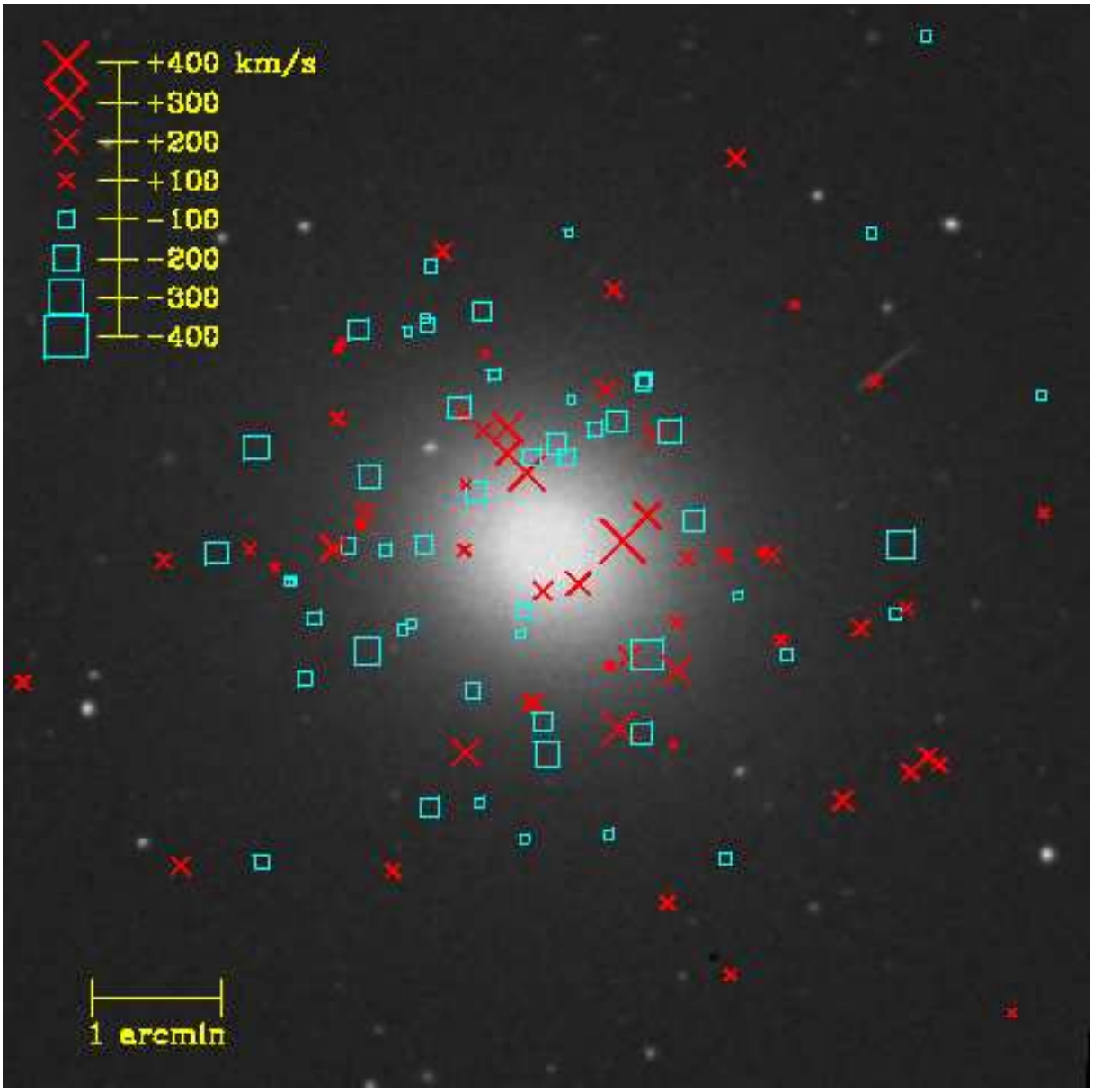

Fig. 1. NGC 3379 with 109 planetary nebula line-of-sight velocities relative to the systemic velocity, as measured with the William Herschel 4.2-m telescope and the PN.S instrument. Red crosses represent receding velocities, and blue boxes are approaching, where the symbol sizes are proportional to the velocity magnitudes. The background image is from the Digitized Sky Survey (*35*), and the field of view is 8.′4×8.′4 = 26×26 kpc = 14×14 $R_{\rm eff}$.

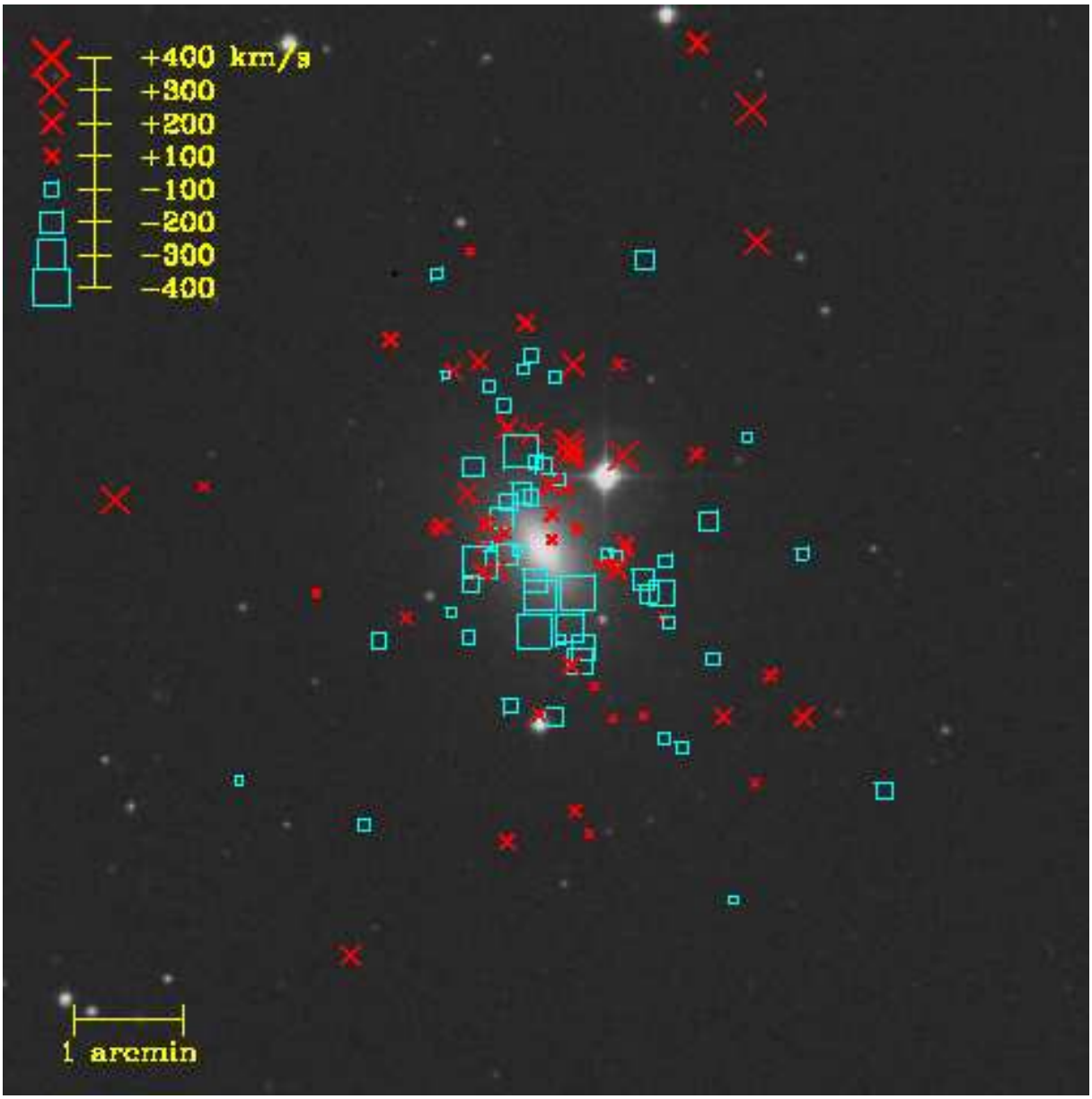

Fig. 2. NGC 821 with 104 planetary nebula velocities. See Fig. 1 for further description. The field of view is $10' \times 10'$= 70×70 kpc = 12×12 $R_{\rm eff}$.

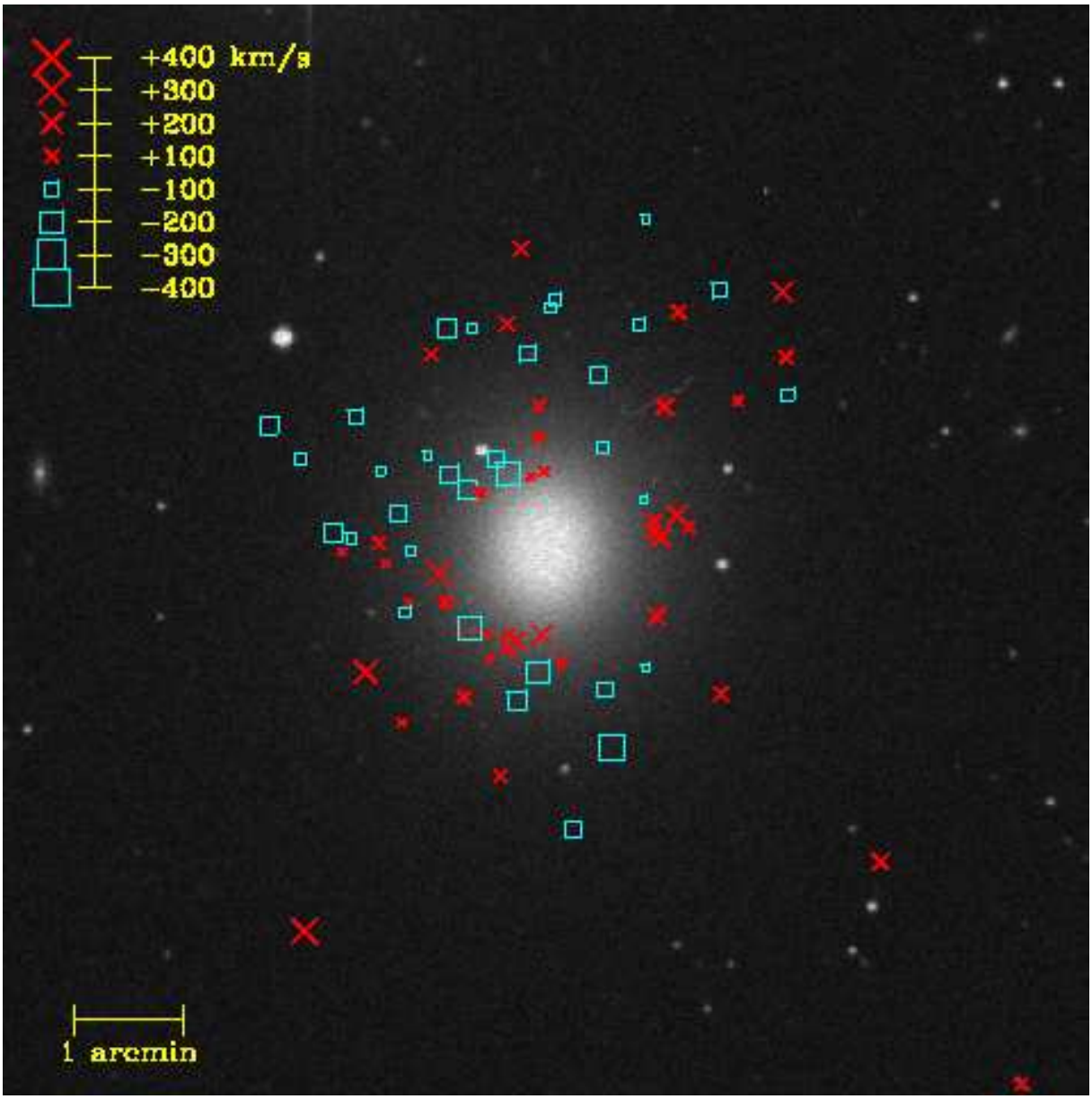

Fig. 3. NGC 4494 with 73 planetary nebula velocities. See Fig. 1 for further description. The field of view is $10' \times 10'$= 50×50 kpc = 12×12 $R_{\rm eff}$.

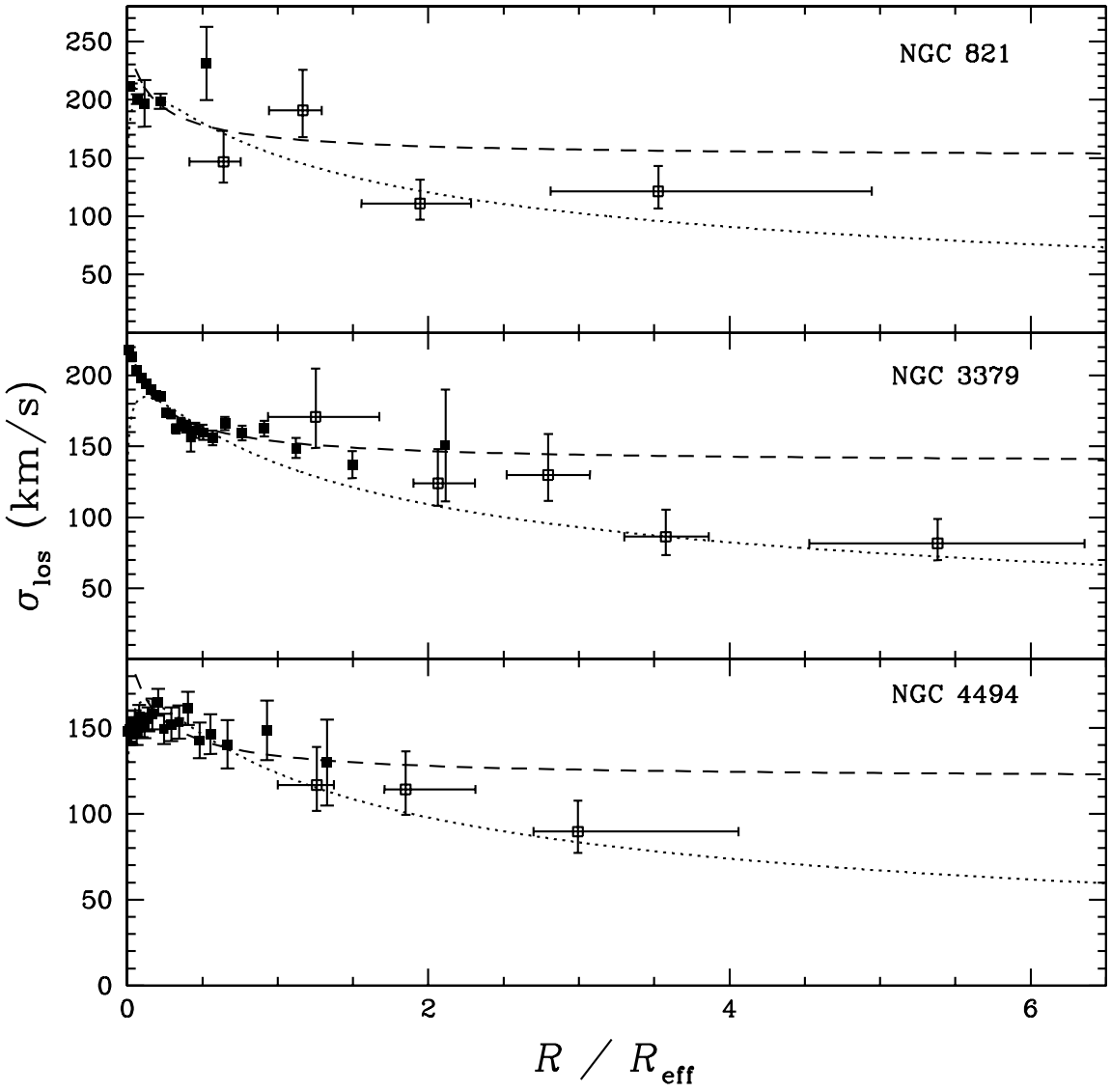

Fig. 4. Line-of-sight velocity dispersion profiles for three elliptical galaxies, as a function of projected radius in units of the effective radius. Open points show planetary nebula data (from PN.S); solid points show diffuse stellar data (*11,12,13*). The vertical error bars show 1 σ uncertainties in the dispersion, and the horizontal error bars show the radial range covered by 68% of the points in each bin. Predictions of simple isotropic models are also shown for comparison: a singular isothermal halo (dashed lines) and a constant mass-to-light ratio galaxy (dotted lines).

Appendix: Methods

Jeans models

The non-rotating spherical Jeans equations link the second moments $\sigma_i(r)$ of a system's velocity distribution to its mass $M(r)$ and luminosity $\nu(r)$ distributions (*36*). We use the formulation

$$M(r) = -\frac{r\sigma_r^2}{G}\left(\frac{d\ln\nu}{d\ln r} + \frac{d\ln\sigma_r^2}{d\ln r} + 2\beta\right), \quad (1)$$

where σ_r^2 and σ_θ^2 are the radial and tangential velocity dispersions, and $\beta \equiv 1 - \sigma_\theta^2/\sigma_r^2$ quantifies the (unknown) velocity anisotropy, We take the luminosity distribution to be the Hernquist (*37*) profile $\nu(r) = L(2\pi r)^{-1}(r+a)^{-3}$ corresponding to the known effective radius of the galaxy ($R_{\rm eff} = 1.8153a$), and parametrize the dispersion profile by the form

$$\sigma_r^2 = v_0^2\left[1 + \left(\frac{r}{r_0}\right)^{\alpha\delta}\right]^{-1/\delta} \quad (2)$$

(thus allowing for a dark halo with a range of radial mass distributions), which is projected and fitted to the dispersion data while optimizing for the parameters $\{v_0, r_0, \alpha, \delta\}$. The anisotropy is set to be constant and is varied between the reasonable extremes of $\beta = -0.5$ (tangential) to $\beta = 0.5$ (radial). We then solve the Jeans equation for the mass profile $M(r)$.

These models are suited to exploring the range of outer galaxy mass profiles, and not for reproducing the fine structure of the dispersion data inside 1 $R_{\rm eff}$. They are thus illustrative of the range of Υ_{B5} associated with the anisotropy uncertainty, and these are the Υ_{B5} values reported in Table 1; the statistical uncertainty is of the same order of magnitude as this systematic uncertainty. As discussed for NGC 3379, the assumption of spherical symmetry should be accurate enough for mass estimates at the 10% level.

Orbit models

Our orbit library method is documented in (*38*). In summary, it begins with an assumed form for the mass distribution, and in its gravitational potential calculates a library of orbits, of all types from radial to circular. These individual orbits are then combined non-parametrically to find the best fit to the observational constraints. Regularization is used to stabilize the solution, but at such a low level as to avoid biasing them. The fit to the data is quantified by a likelihood function $\mathcal{L}$, and 68% confidence limits in model parameters are given by $\Delta\ln\mathcal{L} = 1/2$. Because the degrees of freedom are ill-defined with this method, the absolute value of $\ln\mathcal{L}$ is not very informative, but the diffuse stellar component of the fits (photometric and kinematic) has a typical $\chi^2 = 8$–9 for 129 data points, and the models qualitatively reproduce the data properties.

We use a grid of models consisting of a constant mass-to-light ratio Hernquist model galaxy (*37*) plus a CDM simulated dark halo (*26*), with the mass density distribution:

$$\rho(r) = \frac{v_*^2 a^2}{2\pi G r (r+a)^3} + \frac{v_s^2 r_s}{4\pi G r (r_s+r)^2}. \quad (3)$$

The mass model parameters are thus the halo core radius r_s, the mass of the stars v_*^2, and the relative masses of the stars and halo v_s^2/v_*^2. Our grid covers values of r_s from 113″ to 700″ (6 to 36 kpc), v_* from 575 to 625 km s^{-1}, and v_s^2/v_*^2 from 0 to 1.1.

The best-fit solution for NGC 3379 is shown in Fig. A1, and the range of permitted solutions is illustrated by Fig. A2. We find Υ_{B5} (in solar units) to be 6.4 ± 0.6 at 185″ (9 kpc), 7.9 ± 1.1 at 270″ (14 kpc), and 32 ± 13 at 2460″ (120 kpc). Allowable solutions within the 68% confidence limits include $\{r_s, v_*, v_s^2/v_*^2\}$ = {199″, 603, 0.15}, {280″, 610, 0.15}, {350″, 610, 0.12}, {350″, 603, 0.20}, {500″, 610, 0.12}, {500″, 603, 0.20}, and {500″, 603, 0.30}, where v_* is in km s^{-1}.

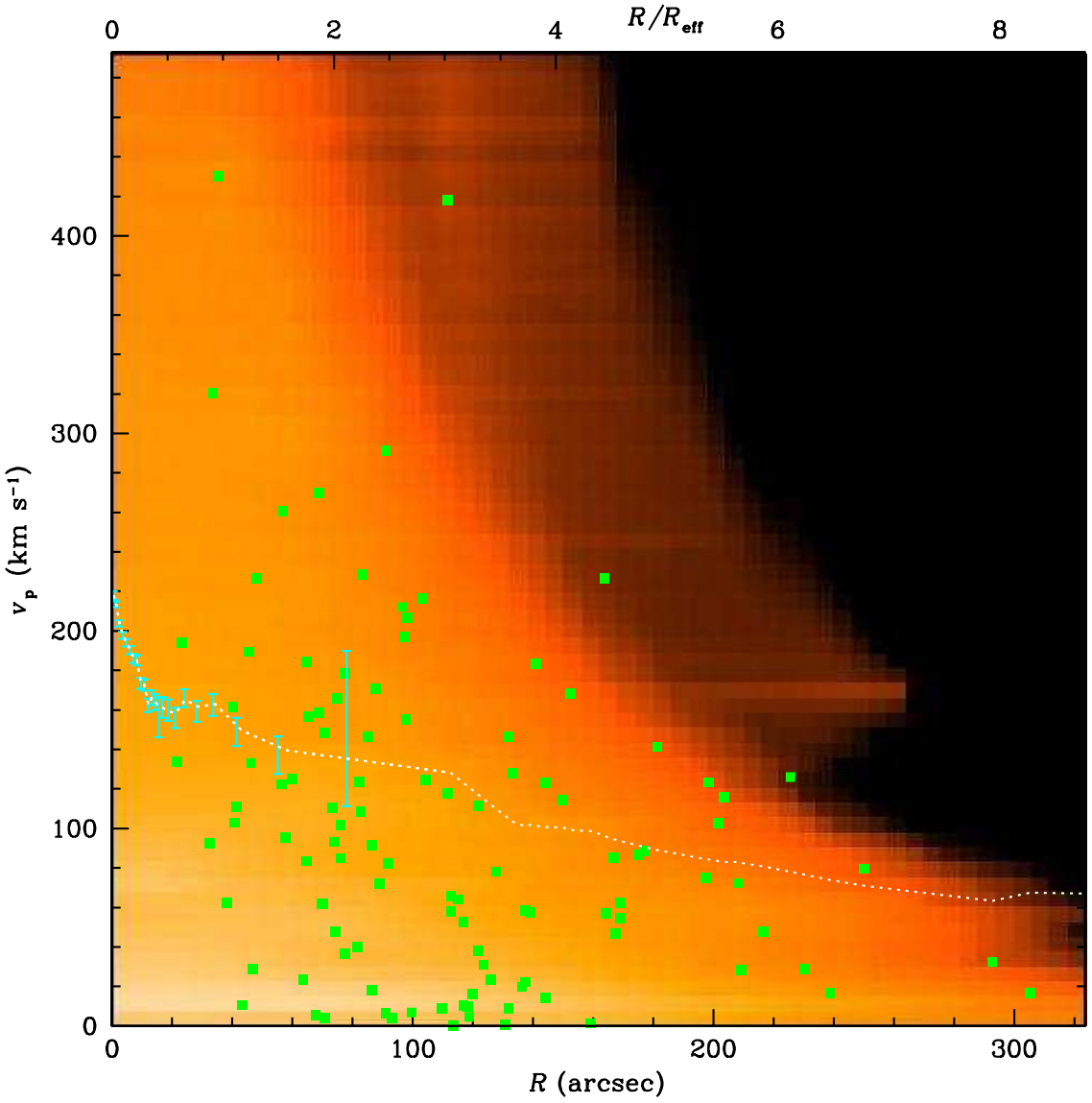

Fig. A1. Line-of-sight velocity distribution with radius in NGC 3379. The error bars show stellar dispersion data (*12*); the points show the PN velocity data. The background shading shows the projection of the best-fit model, multiplied by the stellar luminosity at each radius; the dotted line shows its dispersion.

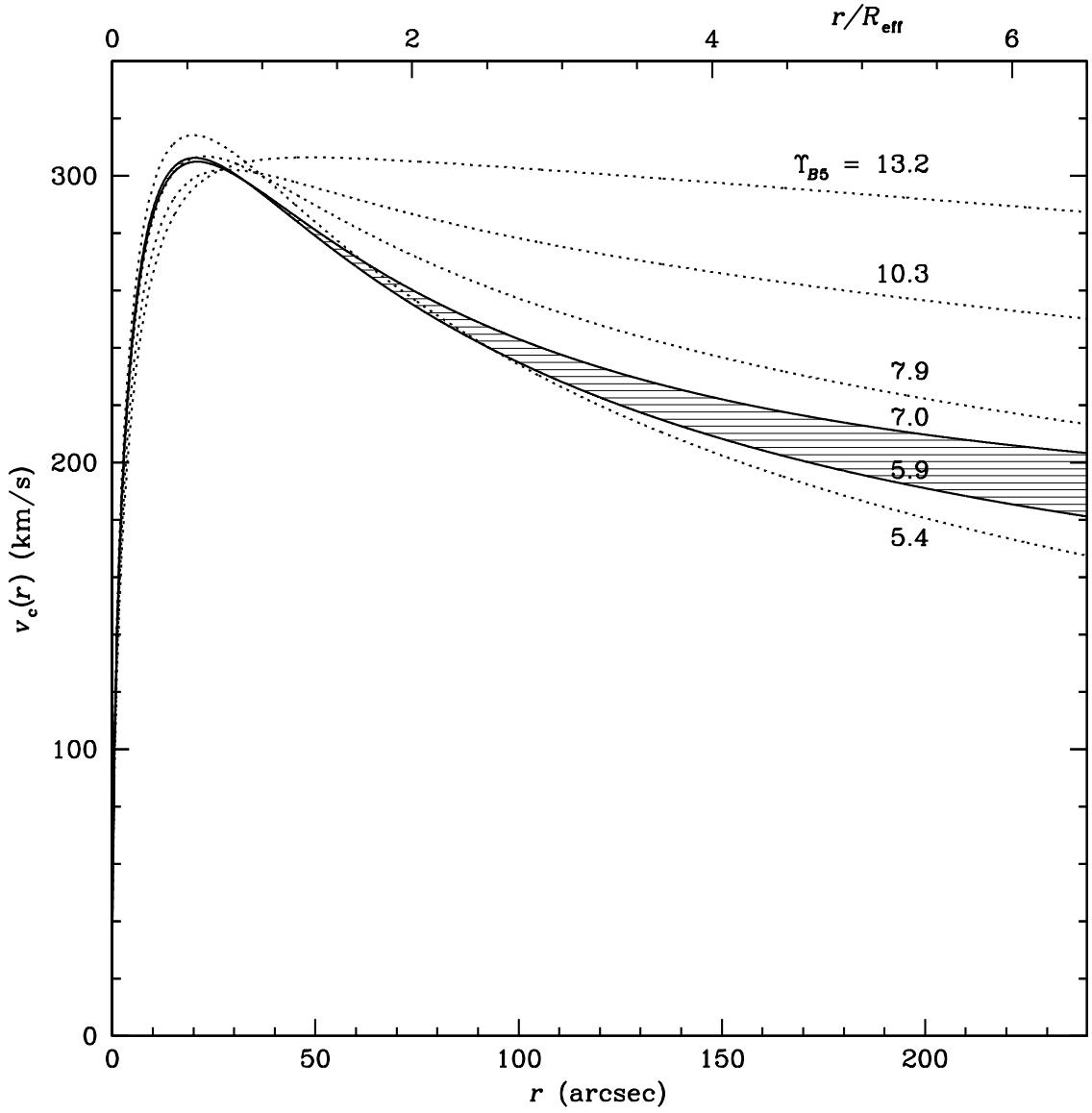

Fig. A2. Intrinsic circular velocity profile with radius, $v_{\rm c}(r) \equiv \sqrt{GM(r)/r}$, of NGC 3379. The solid lines and shaded area show the region permitted by orbit modeling. The dotted lines show models which are ruled out at the 1-σ level: the bottom one shows a constant mass-to-light ratio (M/L) model, the upper three show models with more dominant dark halos. Each model is labeled with its *B*-band mass-to-light ratio (in solar units) at 5 effective radii. Thus we see that the shape of $v_{\rm c}(r)$ for a constant M/L galaxy falls slightly outside the allowed range.